Prolonged and efficient near-infrared photoluminescence of a sensitized organic ytterbium-containing molecular composite.

Chen Lyu[1], Hongfei Li[1], Peter B. Wyatt[3] and William P. Gillin[1,2,*], Huanqing Ye[2,1,*]

1 Materials Research Institute and School of Physics and Astronomy, Queen Mary University of London, Mile End Road, London E1 4NS, United Kingdom

2 Chromosol Ltd, The Walbrook Building, 25 Walbrook, London, EC4N 8A, United Kingdom

3 Materials Research Institute and School of Biological and Chemical Sciences, Queen Mary University of London, Mile End Road, London E1 4NS, United Kingdom

Content

1. Materials and Methods

1) Co-doped $[Yb(F\text{-}TPIP)_3]_x[Zn(F\text{-}BTZ)_2]_{1-x}$ thin film fabrication

The $Yb(F\text{-}TPIP)_3$ and $Zn(F\text{-}BTZ)_2$ were synthesised according to previously reported methods[1,2] and purified using a vacuum train sublimation system. To grow a co-doped thin film, $Yb(F\text{-}TPIP)_3$ and $Zn(F\text{-}BTZ)_2$ are placed in two individual crucibles in a high-vacuum thermal deposition system (a Kurt J. Lesker SPECTROS deposition system). The deposition rates of $Yb(F\text{-}TPIP)_3$ and $Zn(F\text{-}BTZ)_2$ are monitored by independent crystal thickness sensors. The film thickness is calibrated using a stylus surface profilometer. The mole fraction of $Yb(F\text{-}TPIP)_3$ (A) in the mixture with $Zn(F\text{-}BTZ)_2$ (B) is determined by the equation below:

$$c_A = \frac{T_A \times \rho_A / M_A}{T_A \times \rho_A / M_A + T_B \times \rho_B / M_B} \quad (1)$$

M is the molecular weight of a material, ρ is the density of a material and T is the thickness for each component. To have the same absorbance at 405 nm, we co-doped the same absolute $Zn(F\text{-}BTZ)_2$ concentration for these films.

The composite films are covered with a 100 nm thermally-deposited aluminium (Al) layer. Although it is found that the Al layer cannot fully stop hydrogen-containing impurities penetrating materials, this layer is found to be effective in preventing the $Zn(F\text{-}BTZ)_2$ triplet excitons from oxygen quenching. That allows us to measure long-lived phosphorescence of co-doped $Zn(F\text{-}BTZ)_2$ successfully in air at room temperature (RT), which will be discussed later.

2) Analyses of time-resolved PL spectra

Each time-resolved PL (TRPL) spectrum is obtained by averaging 255 time-acquisitions. The lifetime is obtained using a multi-exponential function to fit the TRPL data, shown below:

$$I = I_0 + \sum_1^n A e^{-\frac{t}{\tau_n}} \quad (2)$$

The iteration algorithm of the fitting is Levenberg Marquardt; the quality of the fit is decided by *R*-squared. The uncertainty of the fitting is given by the standard deviation of the lifetime values obtained from between five to ten measurements.

3) Pulse width control

A TG5011 TTL wave generator is used to modulate a Vortran 405nm diode laser to vary the photoexcitation pulse width from 0.05 ms to 5 ms.

4) Excitation spectra measurement

An arc lamp was used to provide a wavelength-tuneable photoexcitation source for the excitation measurement. The excitation wavelength was tuned by dispersing the light using a spectrometer (Triax 180). The monochromatic light from the exit of the Triax 180 was used to illuminate the sample. The PL of the sample was collimated to another spectrometer (Triax 550). The uncorrected excitation spectrum was collected at a fixed PL wavelength whilst scanning the excitation wavelength. The obtained excitation spectrum was then corrected for the arc lamp intensity on the sample.

5) Temperature dependent TRPL measurement

A liquid nitrogen cooled Oxford Instruments cryostat was used to measure the TRPL at low temperature. The temperature of the sample was varied in steps of 10 K from 300 K to 80 K.

2. TRPL spectra under vacuum

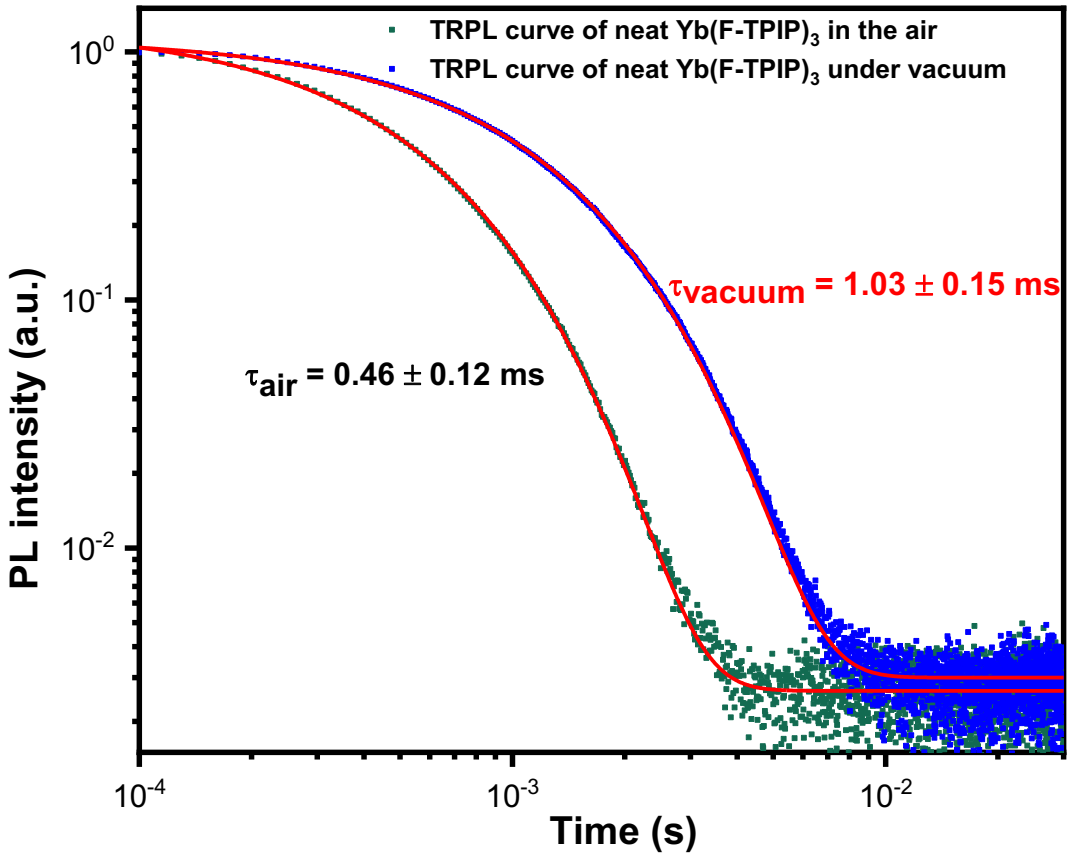

Figure S1. Time-resolved PL spectra of a neat Yb(F-TPIP)$_3$ film at an emission wavelength of 975 nm. The time-resolved PL spectra were recorded by directly exciting Yb^{3+} ions using a ~7 ns laser pulse at 940 nm. The green dots show the TRPL curve when the sample was placed in air and the blue dots show the TRPL curve when the sample was placed under vacuum (5×10^{-5} mbar).

A single exponential fitting gives an Yb^{3+} emission lifetime (τ_{PL}) of 0.47 ± 0.05 ms when the film was placed in air which increases to 1.03 ± 0.04 ms in a vacuum of 10^{-5} mbar. With a measured intrinsic radiative lifetime (τ_{rad}) of ~ 1 ms for excited Yb^{3+} ions in Yb(F-TPIP)$_3$,[3] the IQE of the Yb^{3+} emission in our measurements is ~ 47% with the sample in air, while the IQE reaches ~ 100% with the sample under vacuum. The difference in lifetimes suggest that highly volatile quenching centres are responsible, and the most probable source of this quenching is water vapour which must be able to rapidly penetrate the film to form local

quenching centres. This result indicates that there is no significant self-quenching of the Yb^{3+} ions and the realization of ~ 100% IQE only needs an effective encapsulation of the film samples.

3. PL spectrum of $[Y(F\text{-}TPIP)_3]_{0.5}[Zn(F\text{-}BTZ)_2]_{0.5}$ co-doped film

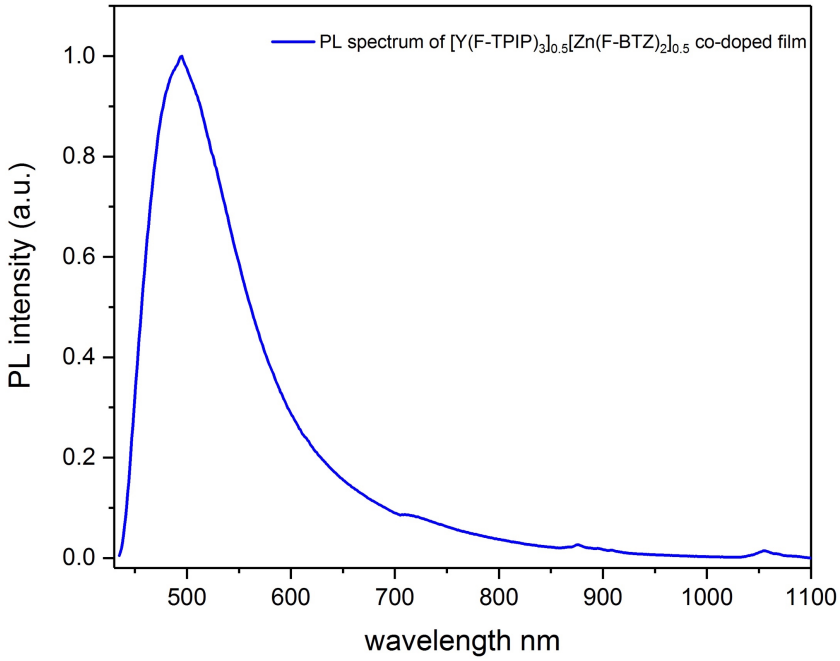

Figure S2. PL spectrum of $[Y(F\text{-}TPIP)_3]_{0.5}[Zn(F\text{-}BTZ)_2]_{0.5}$ co-doped film. *The spectrum is corrected for the optical response of the photon detector and spectrometer grating. The peaks at 890 nm and 1060 nm are due to trace Nd impurities (<0.001%) which are present in the $YCl_3{\cdot}(H_2O)_6$ used to make the $Y(F\text{-}TPIP)_3$.*

The PL spectrum of $[Y(F\text{-}TPIP)_3]_{0.5}[Zn(F\text{-}BTZ)_2]_{0.5}$ co-doped film is shown Figure S2. In the composite film, the thickness of $Y(F\text{-}TPIP)_3$ is 310 nm and the thickness of $Zn(F\text{-}BTZ)_2$ is 100 nm. Since Y^{3+} ions are non-emissive, the broad emission band in Figure S1 results from the $Zn(F\text{-}BTZ)_2$ luminescence only.

4. TRPL spectra at 80K

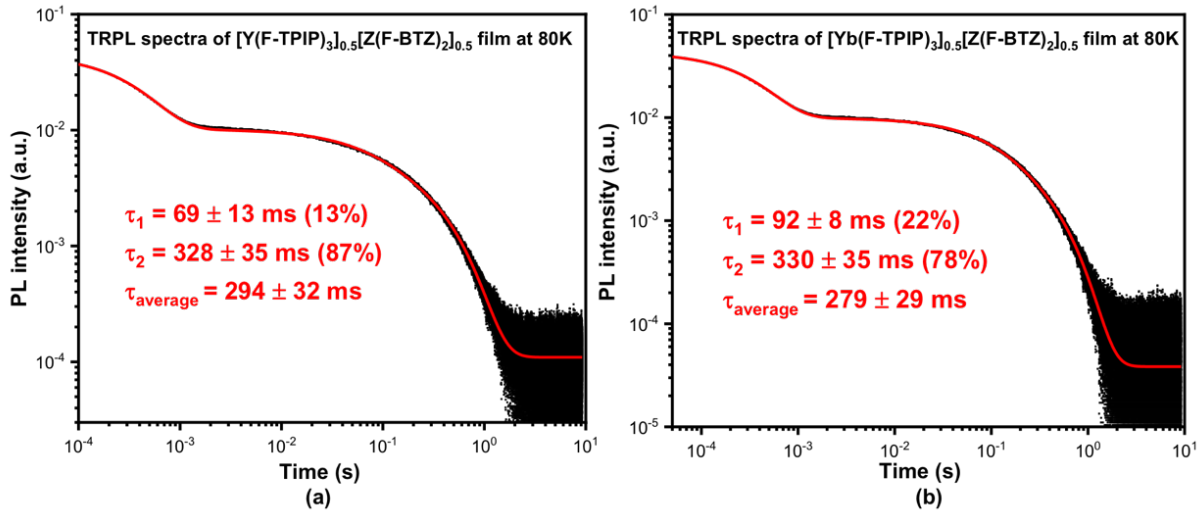

Figure S3. TRPL spectra at 80K. (a) TRPL spectra of $[Y(F\text{-}TPIP)_3]_{0.5}[Zn(F\text{-}BTZ)_2]_{0.5}$ film. (b) TRPL spectrum of $[Yb(F\text{-}TPIP)_3]_{0.5}[Zn(F\text{-}BTZ)_2]_{0.5}$ film. *These spectra at recorded at 560 nm, under 405 nm diode laser excitation. A cryostat is used to cool down the samples to 80K. Black dots indicate the measured TRPL data, red curves represent the fitted decay curves.*

5. Modelling of the energy transfer mechanism

1) Energy transfer scheme

The energy transfer scheme between the energy donor $Zn(F\text{-}BTZ)_2$ and acceptor $Yb(F\text{-}TPIP)_3$ is shown in Figure S3: S_1 and T_1 indicate the singlet and triplet states, Yb_1 represents the $Yb^{3+}\ ^2F_{5/2}$ energy level, R_P is the excitation pump rate, R_S is the singlet state decay rate, R_T is the triplet state decay rate, R_{Yb} is the $Yb^{3+}\ ^2F_{5/2}$ energy level decay rate, R_{ISC} is the inter-system crossing rate, R_{ETS} is the energy transfer rate from S_1 and R_{ETT} is the energy transfer rate from T_1. The singlet and triplet states of the (F-TPIP) ligand can be ignored as they are at an energy of ~4 eV and hence beyond the excitation range used in this work[1-4].

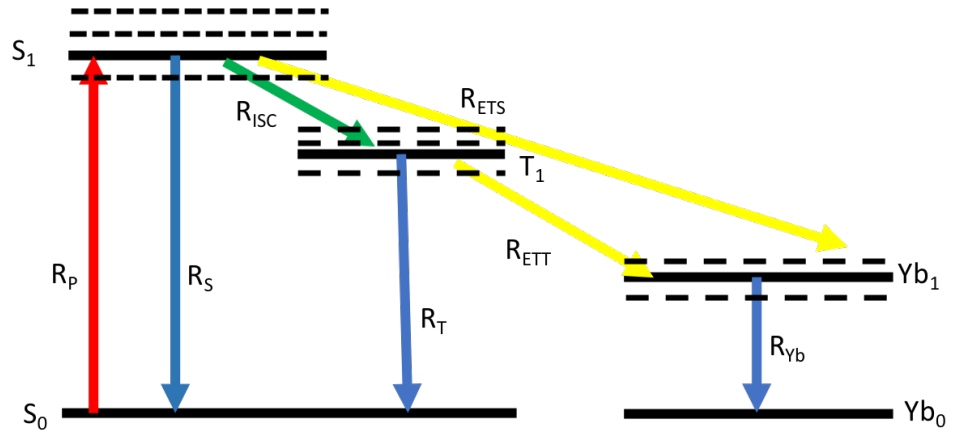

Figure S4. Energy transfer scheme

2) Values of the parameters

Pump rate:. The laser beam spot is focused down to ~ 1 mm^2 on the film sample and the actual laser power on the sample was measured using a photodiode detector (Newport UV818). With a power density of the excitation pulse of 1 ± 0.1 W/cm^2 the photon flux ρ, is 2.03 ± 0.21×10^{18} $cm^{-2}s^{-1}$. $Zn(F\text{-}BTZ)_2$ is dissolved in DMSO to measure its absorbance; the calculated absorption cross-section σ is 1.67±0.3×10^{-16} cm^2. Hence, the pump rate R_P is calculated by $\rho \times \sigma$ to give 341 ± 6 s^{-1} as the pump rate, at 1 W/cm^2, for this modelling.

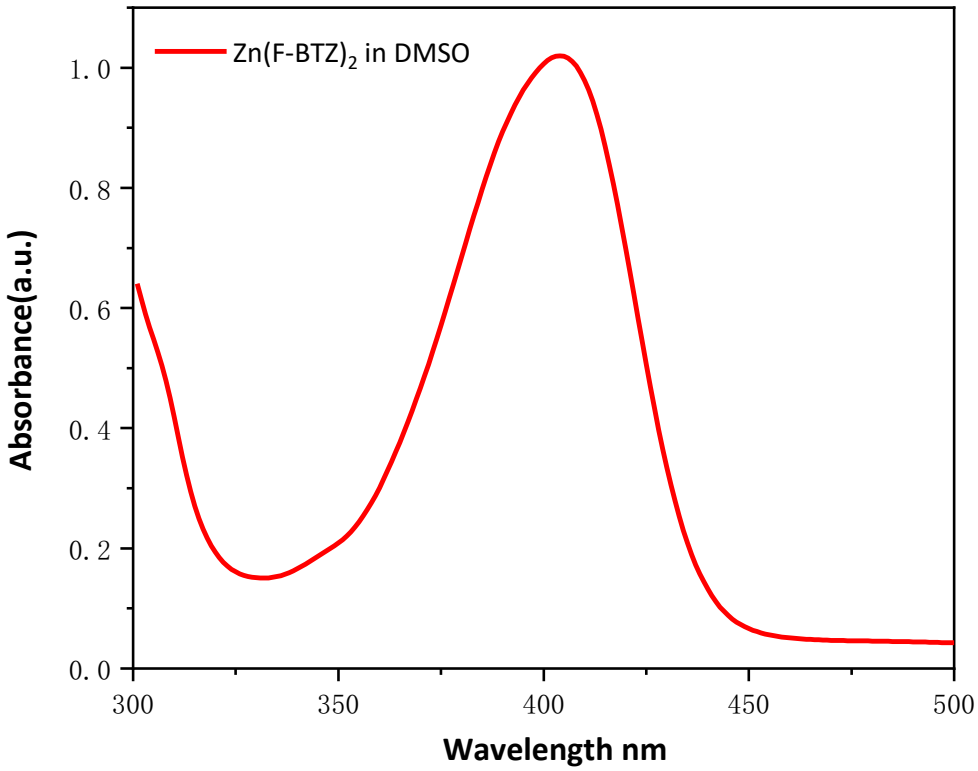

Figure S5. Absorption spectrum of Zn(F-BTZ)$_2$. *Zn(F-BTZ)$_2$ is dissolved in DMSO solvent. The molar concentration of the solution is 9.8×10^{-7} M.*

***R_S* and *R_{ISC}*:** The intersystem crossing rate R_{ISC} is obtained from our previous published work[4] in which the R_{ISC} is fitted by modelling the temperature-dependent ratio of fluorescence and phosphorescence; the calculated value is 3.7×10^{7} s^{-1}. The measured singlet lifetime for the powder is shown in Figure S5, giving a decay rate with $R_s = \sim 2 \times10^{8}$ s^{-1}. This is comparable to that measured in the composite film.

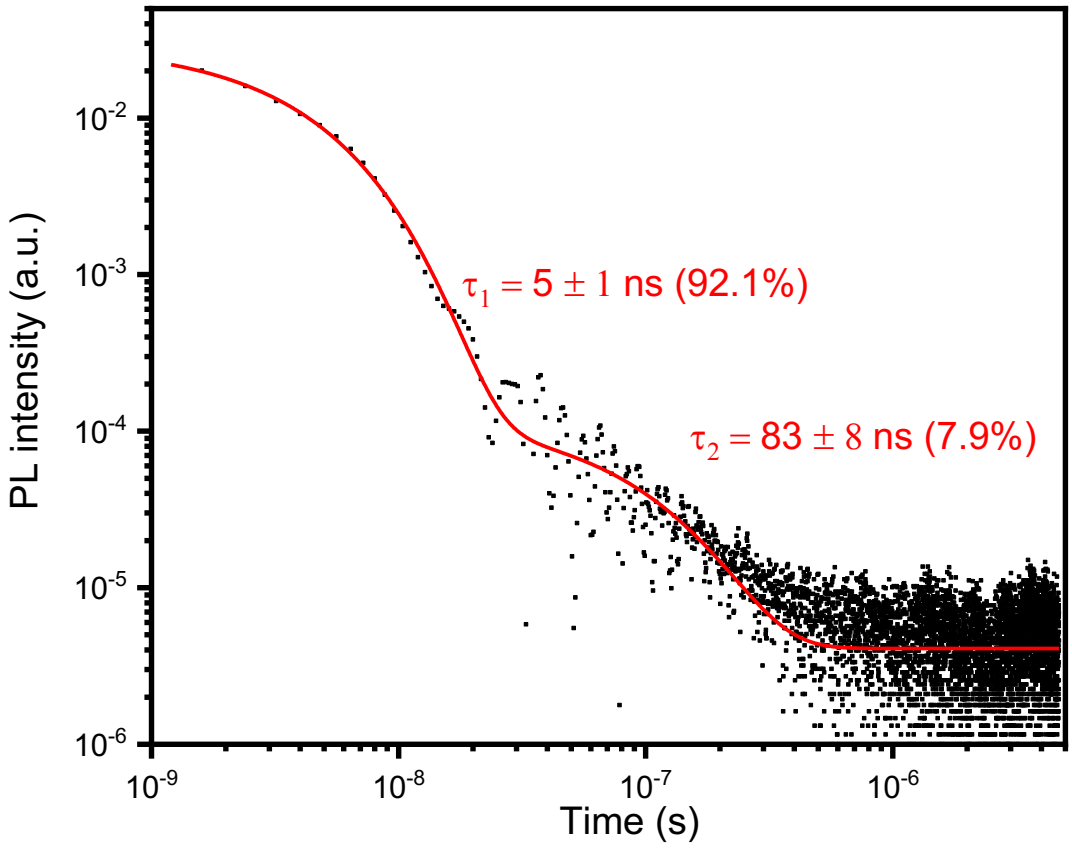

Figure S6. Time-resolved PL spectrum of pure Zn(F-BTZ)$_2$ power at 500 nm. *The powder is excited by a nanosecond pulse Nd:YAG laser. Red curve indicates the exponential fitting results of the decay process. The average lifetime gives the singlet decay rate.*

R_T and the estimation of R_{ETT}: The experimentally measured triplet lifetime is affected by the triplet intrinsic decay rate R_T, triplet energy transfer rate R_{ETT}, and any other nonradiative decay rate R_{NR}: $\tau_T = \frac{1}{R_T+R_{NR}+R_{ETT}}$. Thus, if we replace Yb^{3+} ions with Y^{3+} ions which have no dipole-dipole coupling with the $Zn(F\text{-}BTZ)_2$ excitons, the difference of the triplet lifetime would be solely due to the energy transfer from triplet to Yb^{3+}. The measured TRPL spectra of $[Yb(F\text{-}TPIP)_3]_{0.5}[Zn(F\text{-}BTZ)_2]_{0.5}$ film and $[Y(F\text{-}TPIP)_3]_{0.5}[Zn(F\text{-}BTZ)_2]_{0.5}$ film at a wavelength of 600 nm are shown in Figure S6. Given the overall decay rates of the co-doped films as R_{Yb_600nm} = ~163 ± 35 s^{-1} and R_{Y_600nm} = 187 ±31, the difference between R_{Yb_600nm} and

R_{Y_600nm} is within the experimental error. So, we use the error bar of ~35 s^{-1} as an estimation of the largest energy transfer rate we can achieve.

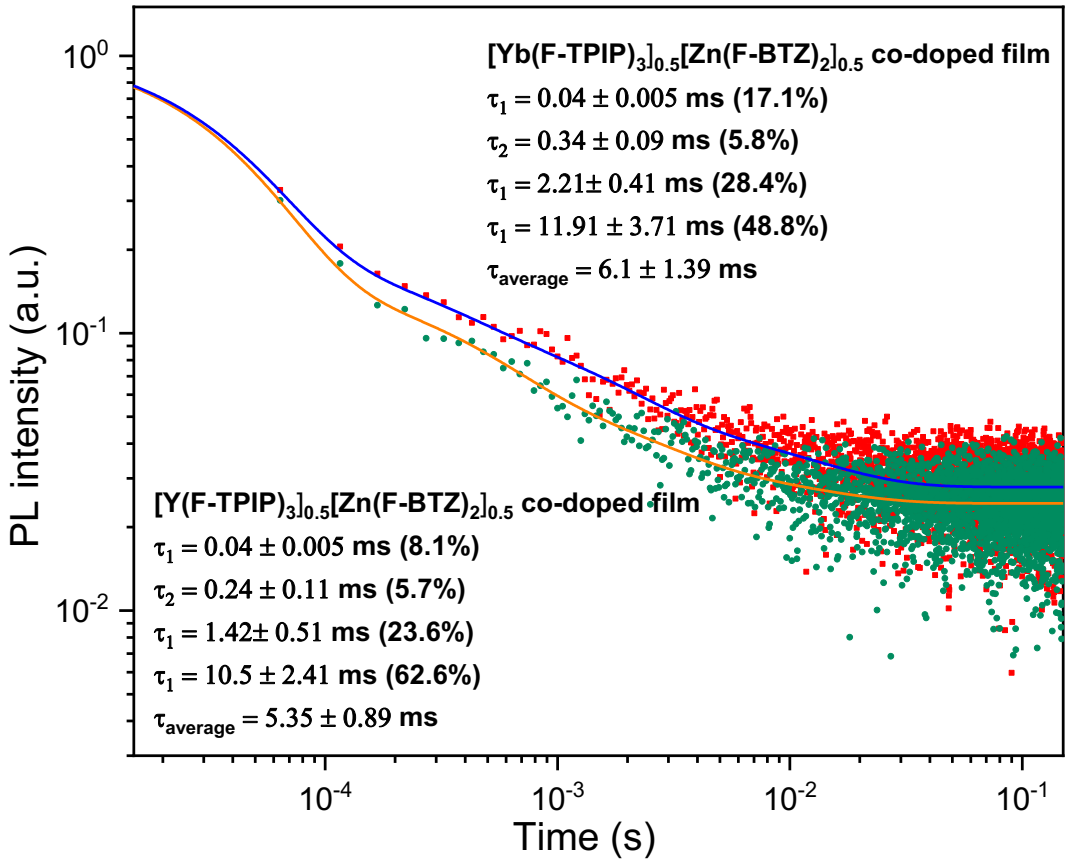

Figure S7. Time-resolved PL spectra of $[Yb(F\text{-}TPIP)_3]_{0.5}[Zn(F\text{-}BTZ)_2]_{0.5}$ and $[Y(F\text{-}TPIP)_3]_{0.5}[Zn(F\text{-}BTZ)_2]_{0.5}$ films at 600 nm. *The TRPL spectrum are collected under a 2.3 Hz square wave modulated 405 nm diode laser excitation. The red and green dots indicate the decay curve of $[Yb(F\text{-}TPIP)_3]_{0.5}[Zn(F\text{-}BTZ)_2]_{0.5}$ films and $[Yb(F\text{-}TPIP)_3]_{0.5}[Zn(F\text{-}BTZ)_2]_{0.5}$, respectively.*

3) Rate equations for the modelling

The rate equation modelling includes two phases: the excitation laser pulse is either on or off. When the laser is on, the photoexcitation continues to populate the singlet states, triplet states and the Yb^{3+} $^2F_{5/2}$ level. Once the laser is cut off, the population in the excited states

starts to relax to the ground state. The experimentally measured TRPL spectra was recorded by triggering the timing when the excitation laser pulse is cut off.

When the laser pulse is on: In this case, the energy transfer between Zn(F-BTZ)$_2$ and Yb(F-TPIP)$_3$ relies on the Förster resonant energy transfer (FRET) in which the energy transfer rate depends on the dipole-dipole coupling. That suggests there are no electron exchanges between the donor and accepter; thus, the electrons are conserved in Zn(F-BTZ)$_2$ and Yb(F-TPIP)$_3$ separately. It is noted that we do not consider the bleaching effect when the Yb^{3+} $^2F_{5/2}$ energy level reaches population inversion. Thus, this model is only suitable when the population at Yb^{3+} excited states are low. Based on the assumptions above, the rate equations can be listed as shown below:

$$\frac{\mathrm{d}N_{S1\_on}[t]}{\mathrm{d}t} = R_P \times \left(N_{Zn\_on}[t] - N_{s1\_on}[t] - N_{T1\_on}[t]\right) - N_{S1\_on}[t] \times (R_S + R_{ISC} + R_{ETS})$$

(3)

$$\frac{\mathrm{d}N_{T1\_on}[t]}{\mathrm{d}t} = N_{S1\_on}[t] \times R_{ISC} - N_{T1\_on}[t] \times (R_T + R_{ETT})$$

(4)

$$\frac{dN_{Yb1\_on}[t]}{\mathrm{d}t} = N_{S1\_on}[t] \times R_{ETS} + N_{T1\_on}[t] \times R_{ETT} - N_{Yb1\_on}[t] \times R_{Yb}$$

(5)

$$N_{S1\_on}[0] = 0$$

(6)

$$N_{T1\_on}[0] = 0$$

(7)

$$N_{Yb1\_on}[0] = 0$$

(8)

$$N_{groud}[t] = N_{Zn\_on}[t] - N_{s1\_on}[t] - N_{T1\_on}[t]$$

(9)

In the rate equations above, N_{ground} represents the total number of excited state population, N_{Zn} indicates the overall population of the $Zn(F\text{-}BTZ)_2$ chromophore.

When the laser pulse is switched off: Once the excitation laser pulse is off, the pump rate is set as 0, therefore we can list the rate equation at the laser-off stage:

$$\frac{dN_{S1\_off}[t]}{dt_2} = -N_{S1\_off}[t_2] \times (R_S + R_{ISC} + R_{ETS}) \quad (10)$$

$$\frac{dN_{T1\_off}[t]}{dt_2} = N_{S1\_off}[t_2] \times R_{ISC} - N_{T1\_off}[t_2] \times (R_T + R_{ETT}) \quad (11)$$

$$\frac{dN_{Yb1\_off}[t]}{dt_2} = N_{S1\_off}[t_2] \times R_{ETS} + N_{T1\_off}[t_2] \times R_{ETT} - N_{Yb1\_off}[t_2] \times R_{Yb} \quad (12)$$

$$t_2 = t - t_{laser\ pulse\ length} \quad (13)$$

$$N_{S1\_off}[0] = N_{S1\_on}\left[t_{laser\ pulse\ length}\right]$$

(14)

$$N_{T1\_off}[0] = N_{T1\_on}\left[t_{laser\ pulse\ length}\right]$$

(15)

$$N_{Yb1\_off}[0] = N_{Yb1\_on}\left[t_{laser\ pulse\ length}\right]$$

(16)

The analytical solution in Equation (17) indicates the decay of Yb^{3+} $^2F_{5/2}$ energy level population:

$$N_{Yb1\_off}[t_2] = -\left(\frac{R_{ETS}}{R_{ETS}+R_S-R_{Yb}}\right) \times e^{-(R_{ETS}+R_S)\times t_2} + \left(\frac{N_{S1\_on}[t_{laser\ pulse\ length}]\times R_{ETS}}{R_{ETS}+R_S-R_{Yb}} + \frac{N_{T1\_on}[t_{laser\ pulse\ length}]\times R_{ETT} + N_{Yb1\_on}[t_{laser\ pulse\ length}]\times(R_{Yb}-R_{ETT}-R_T)}{R_{Yb}-R_{ETT}-R_T}\right) \times e^{-R_{Yb}\times t_2} + \left(\frac{R_{ETT}}{R_{Yb}-R_{ETT}-R_T}\right) \times e^{-(R_{ETT}+R_T)\times t_2} \quad (17)$$

Equation (17) suggests that after the pulse is switched off there is one exponential rise process and two exponential decay process. The rise process is due to the fast energy transfer from the singlet to Yb^{3+}. The other two-exponential decay processes are attributed to the intrinsic Yb decay rate and the triplet de-excitation rate, respectively. Since the singlet decay

rate is large compared to both the Yb^{3+} decay rate and the energy transfer rate, R_{ETS} the pre-factor will be very small. In addition, the term $-e^{-(R_{ETS}+R_S)\times t_2}$ means this rise process is very fast and beyond the timing resolution of our measurements. We use Equation (18) to calculate the component percentage of the intrinsic Yb decay process and prolonged Yb decay processes so that we can fit it with the measured experimental component percentages of prolonged Yb emission lifetimes η_T, which is shown in Table S1.

$$\eta_T = \frac{\int_0^{+\infty} A_{T1\_off}\times e^{-(R_{RTT}+R_T)\times t_2}}{\int_0^{+\infty} A_{Yb1\_off}\times e^{-R_{Yb}\times t_2}+\int_0^{+\infty} A_{T1\_off}\times e^{-(R_{ETT}+R_T)\times t_2}}$$

(18)

A_{T1_off} and A_{Yb1_off} are the coefficients of the intrinsic Yb^{3+} decay process and prolonged Yb^{3+} decay processes. Least square fitting is used to fit the unknown parameter R_{ETS}. From the fitting, R_{ETS} = ~2.7×10^7 s^{-1}; the error of the least square fitting is $\pm$ 0.3×10^7 s^{-1}.

Power dependent PL: By feeding the fitted singlet energy transfer rate back into the steady-state rate equation as shown in equation (19)

$$N_{Yb1\_Steady} = \frac{N_{Zn}\times\phi_{Zn}\times P\times(R_{ETT}\times R_{ISC}+R_{ETS}\times(R_T+R_{ETT}))}{\phi_{Zn}\times P\times((R_{ISC}+R_{ETT}+R_T)+(R_{ETT}+R_T)\times(R_{ISC}+R_S+R_{ETS}))\times R_{Yb}} \quad (19)$$

The steady-state population of the Yb^{3+} ions can be converted to PL intensity by correcting it with scaling factor L:

$$I_{PL} = N_{Yb1\_steady}\times L \quad (20)$$

Thus, the experimentally measured power dependent curve can be fitted with equation (20), shown in Figure S7.

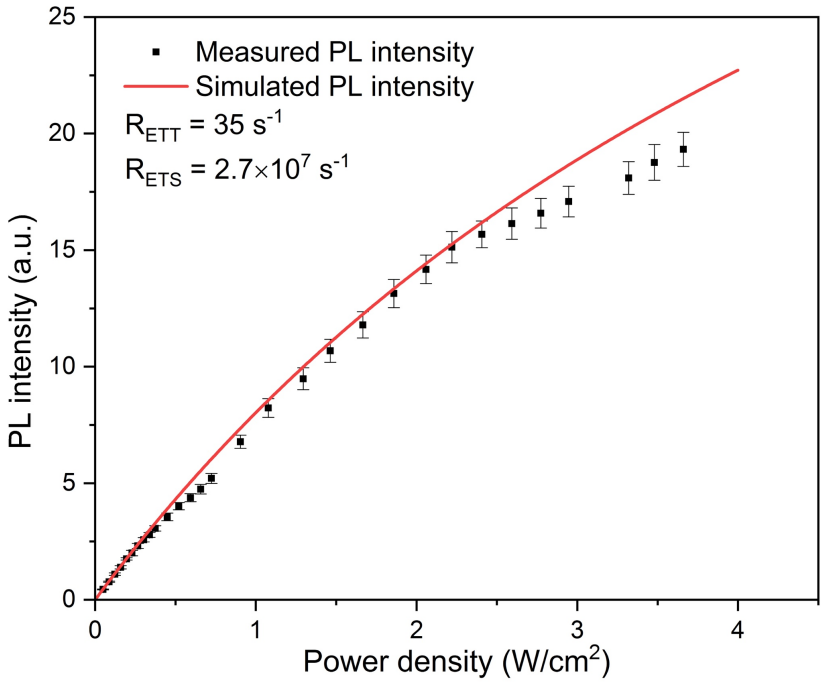

Figure S8. Power dependent PL intensity at 975nm

5. Förster resonant energy transfer (FRET) rate calculation

The Förster resonant energy transfer rate between the energy donor $Zn(F\text{-}BTZ)_2$ and acceptor $Yb(F\text{-}TPIP)_3$ is calculated using equations (21), (22) and (23)[5].

$$R_{FRET} = \frac{1}{\tau_D} \times \left(\frac{R_0}{r}\right)^6 \quad (21)$$

$$R_0{}^6 = 8.79 \times 10^{-5} \times \left(\frac{\kappa^2 \times Q_D}{n^4}\right) \times J(\lambda) \quad (22)$$

$$J(\lambda) = \int F_D(\lambda) \times \varepsilon_A(\lambda) \times \lambda^4 d\lambda \quad (23)$$

In equation (21), τ_D is the donor radiative decay lifetime in the absence of acceptor, R_0 is the Förster radius and r is the distribution distance between molecules. In equation (22), Q_D is the quantum yield of the donor material, n is the refractive index of the composite film, κ^2 is the orientation factor between two coupled dipoles and $J(\lambda)$ is the spectral overlap integral between the donor and acceptor. To calculate $J(\lambda)$, $F_D(\lambda)$ is the donor emission spectrum when the peak intensity is normalized to 1, $\varepsilon_A(\lambda)$ is the molar absorption coefficient of the acceptor and λ is the wavelength. Note that the units of the $\varepsilon_A(\lambda)$, λ and R_0 are not SI units. The unit of $\varepsilon_A(\lambda)$ is $M^{-1}cm^{-1}$ and the unit of wavelength λ is nm; the distances r and R_0 are expressed in Å. The values and units of the parameters used in the calculation are shown in table S1. If we use the commonly used value $\frac{2}{3}$ for κ^2 and give the Q_D with a range from 10% to 100%, with the distribution distance r varying from 7 Å to 10 Å, we can give a reasonable estimate of the range of calculated R_{FRET}. The calculated R_{FRET} shows a maximum value of R_{FRET_max} = ~ 638 s^{-1} when the Q_D =100% and r = 7 Å and a minimum value of R_{FRET_min} = ~ 5 s^{-1} when the Q_D = 10% and distribution distance r = 10 Å, respectively.

Table S1 Value of the parameters for FRET rate calculation

Parameter	τ_D	r	κ^2	Q_D	n	$J(\lambda)$
Value	5.35 ± 0.89 ms	7~10 Å	$\frac{2}{3}$	10%~100%	1.47	$4.5 \pm 0.5 \times 10^{10}$ Å^6

6. Modelling of temperature-dependent prolonged lifetime

The energy transfer scheme that includes the reverse intersystem crossing (RISC) process is shown in figure S8. Based on the modelling in Section 3, the prolonged lifetime is an interpretation of the triplet de-excitation process. Herein, we resolve the measured decay rate to RISC rate R_{RISC} and triplet intrinsic decay rate R_T so that we can we simplify the modelling by simulating the dynamics of excited triplet states.

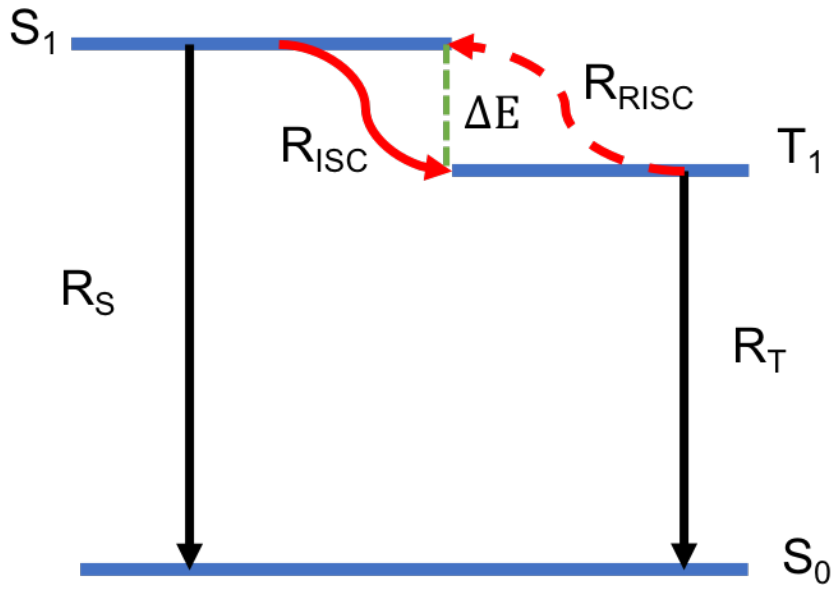

Figure S9. Energy transfer scheme with reversed intersystem crossing process

Assuming a laser pulse with ~330 ms is used to excite the sample and build up the S_1 and T_1 populations. The dynamics of the excited singlet and triplet states can be simulated by equations (24) to (28), shown below:

$$\frac{dN_S[t]}{dt} = -N_S[t] \times R_{ISC} - N_S[t] \times R_S + N_T[t] \times R_{RISC} \quad (24)$$

$$\frac{dN_T[t]}{dt} = -N_T[t] \times R_T - N_T[t] \times R_{RISC} + N_S[t] \times R_{ISC} \quad (25)$$

$$N_S[0] = A \tag{26}$$

$$N_T[0] = B \tag{27}$$

In equation (24) to (27), R_S is the singlet decay rate, R_{ISC} is the intersystem crossing rate (ISC), R_{RISC} is the reversed intersystem crossing rate, A and B are the initial population of S_1 and T_1 state. By solving the rate equations, the decay rate of triplet state is shown below:

$$R_{Simulated} = -\frac{1}{2}\left(R_{ISC} + R_{RISC} + R_S + R_T - \sqrt{{R_{ISC}}^2 + 2R_{RISC}(R_{RISC} + R_S - R_T) + (R_{RISC} - R_S + R_T)^2}\right) \tag{28}$$

In equation (28), the reverse intersystem crossing rate R_{RISC} is dependent on the temperature, shown by equation (29).

$$R_{RISC} = R_{ISC} \times e^{-\frac{\Delta E}{K_B \times T}} \tag{29}$$

ΔE (eV) is the energy gap between S_1 and T_1 states, K_B is the Boltzmann constant (8.6×10^{-5} eV/K). Moreover, the prolonged decay rate ($1/\tau_{Prolonged}$) measured from 80 K to 293 K is shown in Table S3. Thus, using equation (28) and (29) to fit those decay rates, we can obtain the fitted value of ΔE as 0.17 eV with a fitting error of ± 0.02 eV.

7. Lifetime and component percentages

Table S2. Excitation pulse width dependent lifetime and component percentage

Laser pulse width ms	τ_{Yb} µs	η_{Yb}	$\tau_{Prolonged}$ ms	$\eta_{Prolonged}$
0.5	483 ± 40	81.5 %	1.78 ± 0.23	18.4 %
1	405 ± 30	67.9 %	2.11 ± 0.33	32.1 %
2	344 ± 40	57.8 %	2.69 ± 0.43	42.2 %
3	291 ± 50	48.5 %	3.41 ± 0.46	51.5 %
4	262 ± 35	46.6 %	3.16 ± 0.52	53.4 %
5	239 ± 44	45.6 %	3.44 ± 0.31	54.4 %

Table S3. Temperature dependent lifetime and component percentage

Temperature K	τ_{Yb} µs	η_{Yb}	$\tau_{Prolonged}$ ms	$\eta_{Prolonged}$
293	419 ± 31	15.7%	9.7 ± 2.3	84.3%
288	481 ± 43	18.6%	11.5 ± 1.8	81.3%

284	465 ± 43	20.1%	12.4 ± 1.6	79.9%
280	425 ± 37	13.8%	15.0 ± 2.1	86.2%
270	394 ± 41	11.7%	17.9 ± 1.9	88.3%
260	366 ± 33	9.5%	21.3 ± 2.4	90.5%
250	367 ± 40	6.9%	28.4 ± 2.6	93.1%
240	371 ± 39	5.2%	39.1 ± 3.3	94.8%
230	385 ± 45	3.8%	50.1 ± 4.3	96.2%
220	391 ± 52	2.9%	63.9 ± 5.4	97.1%
210	396 ± 33	2.2%	77.1 ± 7.8	97.8%
200	429 ± 37	1.9%	97.3 ± 8.8	98.1%
190	466 ± 43	1.6%	112.4 ± 11.4	98.4%
180	487 ± 44	1.3%	125.7 ± 13.1	98.7%
170	513 ± 61	1.1%	140.6 ± 15.3	98.9%
160	442 ± 53	0.9%	153.0 ± 15.7	99.1%
140	547 ± 70	0.8%	189.7 ± 17.3	99.2%
120	639 ± 74	0.6%	218.9 ± 22.2	99.4%
100	515 ± 51	0.3%	253.9 ± 26.4	99.7%
80	623 ± 75	0.2%	304.7 ± 29.7	99.8%

Reference

[1] Z. Li, A. Dellali, J. Malik, M. Motevalli, R. M. Nix, T. Olukoya, Y. Peng, H. Ye, W. P. Gillin, I. Hernández, P. B. Wyatt, *Inorg. Chem.* **2013**, *52*, 1379.

[2] P. B. Glover, A. P. Bassett, P. Nockemann, B. M. Kariuki, R. Van Deun, Z. Pikramenou, **2007**, 6308.

[3] H. Ye, V. Bogdanov, S. Liu, S. Vajandar, T. Osipowicz, I. Hernández, Q. Xiong, *J. Phys. Chem. Lett.* **2017**, *8*, 5695.

[4] J. Hu, P. B. Wyatt, W. P. Gillin, H. Ye, *J. Phys. Chem. Lett.* **2018**, *9*, 2022.

[5] P. G. Wu, L. Brand, *Anal. Biochem.* **1994**, *218*, 1.